COMMUNICATION

Accessing Three Oxidation States of Cobalt in M_6L_3 Nanoprisms with Cobalt-Porphyrin Walls

P. Thomas Blackburn,[a] Iram F. Mansoor,[a] Kaitlyn G. Dutton,[a] Alexei M. Tyryshkin,[a] and Mark C. Lipke[a]

Nanocages with porphyrin walls are common, but studies of such structures hosting redox-active metals are rare. Pt^{2+}-linked M_6L_3 nanoprisms with cobalt-porphyrin walls were prepared and their redox properties were evaluated electrochemically and chemically, leading to the first time that cobalt-porphyrin nanocages have been characterized in Co^{I}, Co^{II}, and Co^{III} states.

Nanocages[1] assembled from molecular components are of interest for the unique properties that arise from surrounding a small volume of space with a shell of repeating functional units.[2] Early studies focused on the ability of these nanoscopic structures to encapsulate molecular guests,[3] while more recent attention has turned to the development of cages that exhibit increasingly complex functions, including stimuli-responsive behaviour[4] and catalytic activity.[5] Redox-active nanocages[6] are especially promising in this regard since redox changes can alter the charge,[7] spin state,[8] geometry,[9] and/or reactivity of these nanostructures.[10] As a result, there is growing interest in the preparation of redox-active nanocages for use as (electro)catalysts,[10] tunable electronic materials,[8] or hosts that provide control over the uptake and release of guests.[7c-e,9]

Porphyrins are appealing building blocks for functional redox-active nanocages since the redox activity and reactivity of (metallo)porphyrins[11] can be incorporated into and modified by these porous structures.[10] Chang and Cook have examined iron- and cobalt- porphyrin nanocages as electrocatalysts for CO_2 and O_2 reduction,[10] finding in the latter case that product selectivity for O_2 reduction can be controlled by the Co---Co distances enforced by the cages.[10b-d] Likewise, we have found that the 3D arrangement of unmetallated porphyrins in M_6L_3 nanoprisms enables the uptake and trapping of cationic guests in response to reduction/reoxidation of these porphyrin walls.[7c] However, aside from these few studies, the redox properties of porphyrin nanocages are poorly developed, especially considering how numerous such structures are in the literature.[12]

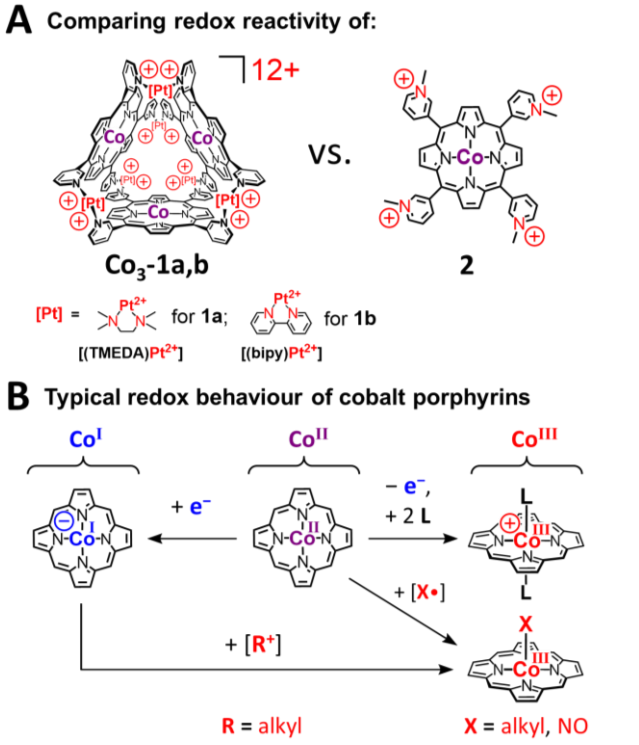

Scheme 1. (A) Cobalt porphyrin nanocages and a monomeric cobalt porphyrin that are compared in this study. (B) Common redox reactivity of cobalt porphyrins complexes.

In this report, we extend our studies of M_6L_3 nanoprisms (L = (3-py)$_4$porphyrin; M = (tmeda)Pt^{2+} for **1a**, (2,2'-bipy)Pt^{2+} for **1b**)[7b,c] to the metalation of their porphyrin walls with cobalt and comparison of the redox properties of the resulting cages **Co_3-1a,b** with those of a monomeric complex [tetrakis(*N*-Me-3-pyridinium)porphyrin]cobalt (**2**, Scheme 1A). As illustrated in Scheme 1B, simple Co^{II} porphyrin complexes, such as **2**, display rich inner- and outer- sphere redox chemistry that provides access to Co^{I} and Co^{III} complexes.[11] Examining these processes in **Co_3-1a,b** led to the first examples of cobalt-porphyrin

[a] *Department of Chemistry and Chemical Biology, Rutgers, The State University of New Jersey, 123 Bevier Road, Piscataway, New Jersey 08854-, United States*

Electronic Supplementary Information (ESI) available. Details of syntheses and experiments. UV-vis, ^{1}H NMR, $^{13}C\{^1H\}$, and DOSY NMR spectra. ESI-MS data. Cyclic voltammograms.

nanocages to be characterized in Co^{I}, Co^{II}, and Co^{III} states, though the cages were found to be more reluctant than **2** to undergo oxidation. This observation reveals an emergent influence of these nanostructures on the redox properties of the cobalt centres, providing insight about how the cages affect the fundamental reactivity of the metalloporphyrins.

The porphyrin walls of **1a**,**b** were metallated with zinc and cobalt by treating the cages with an excess of the respective $M(OAc)_2 \bullet nH_2O$ salt in MeCN (Scheme 2). Metalation with zinc proceeded readily at room temperature, while efficient metalation with cobalt required gentle heating (60 °C). Insertion of M^{2+} ions into the porphyrins was evident from disappearance of the porphyrin NH resonances in the ^{1}H NMR spectra of the cages (Figures S12,13), and from characteristic reductions in the number of porphyrin q-peaks in the UV-vis spectra.[11a,13] The porphyrin walls of **1a**,**b** exhibit four q-peaks,[7b] **Zn_3-1a**,**b** each exhibit two (Figures S71,72), and **Co_3-1a**,**b** each show just one q-peak (Figures S65,66). The q-peaks of **Co_3-1a**,**b** (λ_{max} = 533 and 534 nm, respectively) are similar to that of the monomeric complex **2** (λ_{max} = 534 nm, Figure S59), though the latter exhibits a shoulder (ca. 560 nm) that is less defined in the spectra of **Co_3-1a**,**b**. The ^{1}H NMR spectra of **Zn_3-1a**,**b** are very similar to those of **1a**,**b**,[7b] indicating retention of trigonal prismatic structures in the zinc derivatives (see Figures S22,24). The ^{1}H NMR spectra of **Co_3-1a**,**b** show significant broadening and downfield shifts of some signals due to the paramagnetic Co^{II} centres, but it was possible to identify two pyrrolic CH resonances for each cage (Figures 1 and S12,13), suggesting **Co_3-1a**,**b** also retain the symmetry of the initial, unmetallated structures.

The cages **Co_3-1a**,**b** were further characterized by ESI-HRMS and by EPR spectroscopy, confirming that these derivatives have similar structures to **1a**,**b**. The ESI-HRMS data of **Co_3-1a**,**b** (Figures S46 – S51), like those of **1a**,**b**[7b] and **Zn_3-1a**,**b** (Figures S52 – S57), show a series of peaks with m/z values and isotope patterns corresponding to the charged cages with varying numbers of PF_6^- associated. The EPR spectra of **Co_3-1a**,**b** (Figure S58) recorded at 77 K show rhombic signals (g = 2.400, 2.290, 2.023 for **Co_3-1a**; 2.340, 2.230, 2.023 for **Co_3-1b**) that resolve hyperfine couplings from the ^{59}Co spin (I = 7/2). These spectra are similar to that recorded for **2** (Figure S58), except the signals of the cages have a greater linewidth (9 mT for **Co_3-1a,b**; 5.5 mT for **2**) that is consistent with dipole-dipole coupling between Co^{II} ions at a distance matching that (8 - 9 Å) expected in **Co_3-1a,b**.‡

The redox behaviour of **Co_3-1a**,**b** was evaluated by cyclic voltammetry and compared with that of **2** (Figure 2). The cages and monomeric porphyrin all display reversible Co^{II}/Co^{I} couples at similar potentials ($E_{1/2}$ = −0.98 V, 3e$^-$, **Co_3-1a**; −0.98 V, 3e$^-$, **Co_3-1b**; −0.95 V, 1e$^-$, **2**; all vs. $Fc^{+/0}$). The slightly more positive Co^{II}/Co^{I} couple for **2** vs. **Co_3-1a**,**b** is consistent with our previous observation[7b] that [tetrakis(*N*-Me-3-pyridinium)porphyrin]$^{4+}$ undergoes porphyrin-centred reductions at potentials 50 to 80 mV positive of the reductions of the porphyrins in unmetallated **1a**,**b**. Other reductions of **2** and **Co_3-1a**,**b** are similar to those displayed by [tetrakis(*N*-Me-3-pyridinium)porphyrin]$^{4+}$ and **1a**,**b**,[7b] respectively (Figures S79,81,83). Thus, these processes are attributed to reversible reductions of the 2,2'-bipy ligands in **Co_3-1b**, quasireversible reductions of the pyridinium cations in **2**, and irreversible reductions of the (tmeda)Pt^{2+} linkers in **Co_3-1a**. Cobalt porphyrins should also have accessible Co^{III}/Co^{II} redox couples, but these oxidations could not be observed for **Co_3-1a**,**b** and were only occasionally observed for **2** ($E_{1/2} \approx$ −0.15 V vs. $Fc^{+/0}$, Figure S78). The greater difficulty observing Co^{II} to Co^{III} oxidations for **Co_3-1a**,**b** vs. **2** suggests that it may be harder to access Co^{III} states of the cages, though definitive conclusions cannot be drawn from the CV data since it is generally difficult to observe porphyrin Co^{III}/Co^{II} couples by cyclic voltammetry.[11a]

The redox properties of **Co_3-1a**,**b** and **2** were further probed using a series of inner- and outer- sphere redox reagents. Successful reactions (i.e., forming primarily one well-defined product) are summarized in Schemes 3 and 4. As expected based on CV data, **Co_3-1a,b** and **2** are readily reduced to their

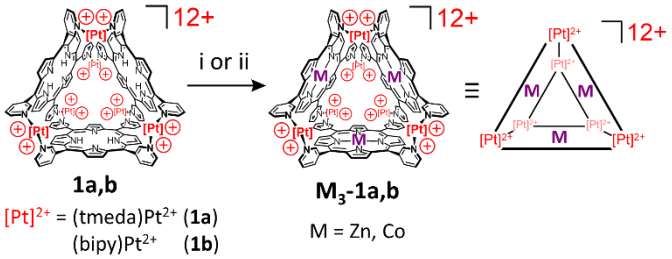

Scheme 2. Metallation of **1a**,**b** with zinc and cobalt. (i) 15 equiv. $Zn(OAc)_2 \bullet 2H_2O$ in MeCN at 23 °C for 16 h. (ii) 15 equiv $Co(OAc)_2 \bullet 4H_2O$ in MeCN at 60 °C for 16 h.

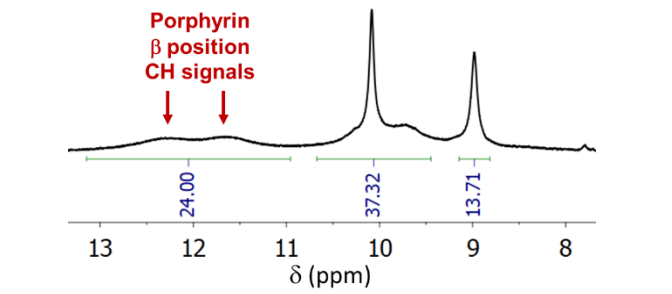

Figure 1. Aromatic region of the ^{1}H NMR spectrum of **Co_3-1a** in CD_3CN (see Figure S12 for full spectrum). The observation of two signals for the pyrrolic CH bonds (β positions) of the porphyrins indicates the trigonal prismatic structure of the cage.

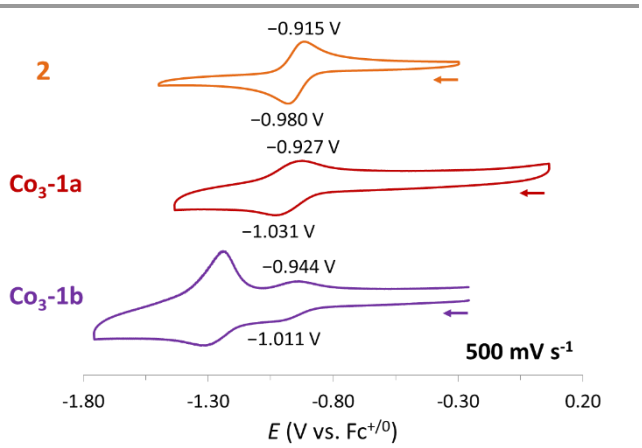

Figure 2. Cyclic voltammograms of **2** (0.1 mM) and **Co_3-1a**,**b** (0.05 mM) recorded in MeCN containing 0.1 M $TBAPF_6$. The peak potentials (E_{pc} and E_{pa}) of the reversible Co^{II}/Co^{I} redox couples are labeled. **Co_3-1b** displays an additional redox process arising from its 2,2'-bipy ligands. Note that currents are not scaled proportionally between each voltammogram.

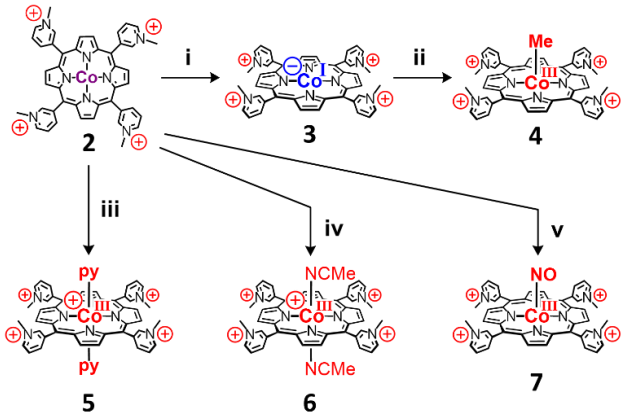

Scheme 3. Redox reactivity of monomeric cobalt porphyrin complex **2** in CD_3CN. (i) 1 equiv. Cp_2Co. (ii) 1 equiv. $[Me_3O]BF_4$. (iii) 2 equiv. pyridine, 3 equiv. $AgPF_6$. (iv) 1 equiv. thianthrenium hexafluorophosphate. (v) 1 atm NO.

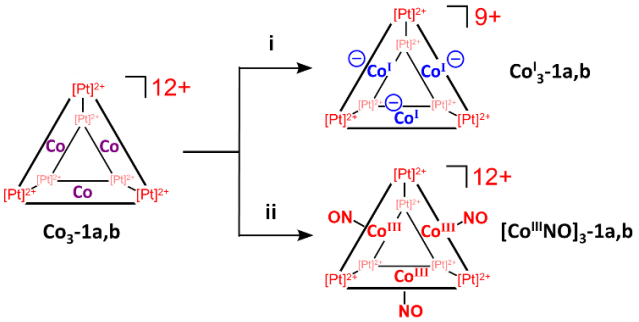

Scheme 4. Redox reactivity of cobalt-metallated nanoprisms **Co$_3$-1a,b** in CD_3CN. (i) 3 equiv. Cp_2Co. (ii) 1 atm NO.

Co^{I} states **Co$^{I}_3$-1a,b** and **3**, respectively, upon treatment with Cp_2Co ($E°$ ≈ −1.3 V vs. $Fc^{+/0}$).[14] The UV-vis spectra of the Co^{I} derivatives all show similar shifts of the Soret bands and q-peaks relative to their Co^{II} states (Figures S60,67,68), consistent with other Co^{I} porphyrin complexes.[11a] Successful reduction of **Co$_3$-1a,b** and **2** was also evident from well-resolved ^{1}H NMR spectra that were observed for the cages and the monomeric porphyrin complex in their diamagnetic Co^{I} states (Figures 3 and S2,16).

Notably, the ^{1}H NMR spectra of **Co$^{I}_3$-1a,b** confirm that the cages maintain trigonal prismatic structures in their reduced states. As shown in Figure 3, the pyrrolic CH resonances of **Co$^{I}_3$-1a** appear as two singlets, consistent with the 2-fold symmetry expected for each porphyrin wall in these structures. Likewise, the *N*CH$_3$ and -CH$_2$- signals of the tmeda ligands are split into two sets for portions of the ligands facing the interior vs. exterior of the cage, as is observed in the ^{1}H NMR spectrum of **1a**.[7b] Diffusion-ordered (DOSY) NMR spectra further support the structural similarity of **Co$^{I}_3$-1a,b** to their unmetallated counterparts (Figures S39,40). To our knowledge, these results represent the first time that NMR spectroscopy has been used to characterize Co^{I} states of nanocages with cobalt-porphyrin walls. The well-resolved ^{1}H NMR spectra obtained for **Co$^{I}_3$-1a,b** suggest that reduction to diamagnetic Co^{I} states may be a generally useful strategy for characterizing nanostructures that include cobalt-porphyrin components.

Following reduction to their Co^{I} states, the accessibility of Co^{III} states of the cages and monomeric porphyrin were examined. Treatment of Co^{I} complex **3** with the CH_3^+ synthon[§,15]

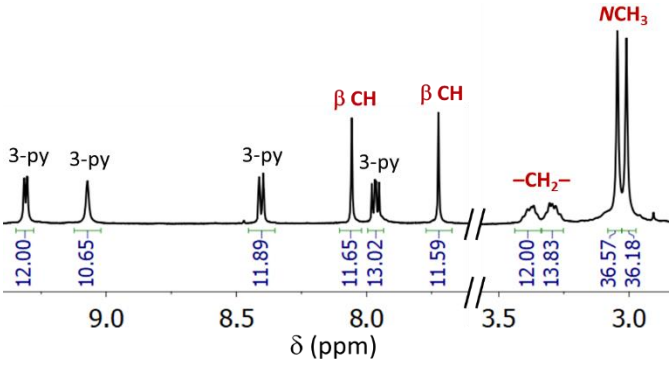

Figure 3. ^{1}H NMR spectrum of **Co$^{I}_3$-1a** prepared in situ in CD_3CN. Red labels are used for signals of the porphyrin and linkers that are desymmetrized by the cage structure.

$[Me_3O]^+$ in CD_3CN resulted in clean oxidative addition to form the Co^{III}–CH_3 complex **4** (Scheme 3), as evident from the appearance of a sharp, upfield ^{1}H NMR singlet at −4.64 ppm (Figure S4).[11c] In contrast, treatment of **Co$^{I}_3$-1a,b** with $[Me_3O]^+$ resulted in the appearance of several upfield ^{1}H NMR signals, spanning from −4.5 to −7.5 ppm (Figures S26,27). Up to six CH_3 resonances might be explained by endo/exo isomerism, but as many as ten CH_3 signals were observed in these experiments. This result, along with other numerous and/or poorly defined NMR signals of the cages after reaction, suggests that the cages do not retain their trigonal prismatic structures upon oxidative addition of CH_3^+ to cobalt. Alternatively, the cages might impose geometric constraints that promote 1 e$^-$ reductive elimination of the Co^{III}–CH_3 groups,[11d] leading to mixed Co^{III}–CH_3/Co^{II} derivatives. Regardless of the underlying reason, tris-[Co^{III}–CH_3] states of the cages could not be accessed cleanly.

Outer-sphere oxidation of **Co$_3$-1a,b** was also more challenging than for **2**. Complex **2** was readily oxidized to a bis-pyridine Co^{III} complex **5** upon treatment with $AgPF_6$ (3 equiv.) and pyridine (2 equiv.) in CD_3CN (Scheme 3, see Figures S6,62 for NMR and UV-vis spectra), while these conditions failed to provide tris-Co^{III} states of either cage. A shoulder at 433 nm did, however, appear on the Soret band (λ_{max} = 412 nm) of each cage (Figure S73,74), suggesting that some of the Co^{II} centres were oxidized to Co^{III}. Steric constraints likely prevent more than one pyridine ligand from coordinating inside the cages, limiting oxidation to just one cobalt site since Ag^+ is not a strong enough oxidant ($E°$ ≈ +0.04 V vs. $Fc^{+/0}$)[14] to access Co^{III} states of the porphyrins unless Co^{III} is stabilized by pyridine ligands.[11a]

Thianthrenium was examined as a stronger oxidant ($E°$ ≈ +0.86 V)[14] for accessing Co^{III} states of the cages. This oxidant provided clean conversion of **2** to a Co^{III} complex **6** (Scheme 3, see Figures S8,63 for NMR and UV-vis spectra), while similar behaviour could not be observed clearly for **Co$_3$-1a,b**. Changes to the UV-vis spectra (Figures S75,76) of each cage confirm that all Co^{II} centres were oxidized, but the resulting ^{1}H NMR spectra (Figures S30,31) show many poorly defined signals, suggesting the trigonal prismatic cage structures are not retained. Since Co^{III} porphyrins often coordinate two axial ligands,[11a,c] steric congestion of MeCN ligands in the interiors of the cages might contribute to structural instability. The electrostatic repulsion of adding three more cationic sites to the already 12+ charged cages might also contribute to their disassembly.

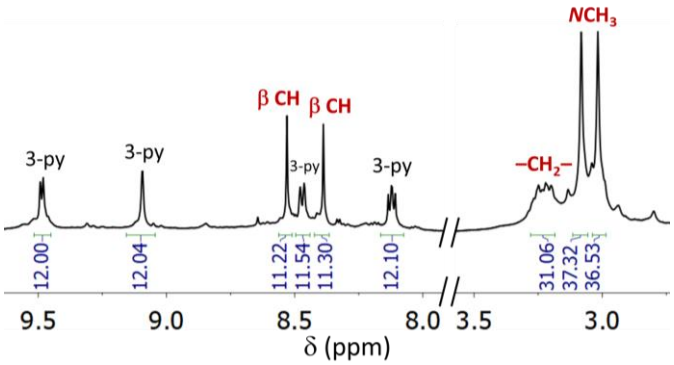

Figure 4. ^{1}H NMR spectrum of [**Co^{III}NO]$_3$-1a** prepared in situ in CD_3CN. Red labels are used for porphyrin and linker signals that are desymmetrized by the cage structure.

Nitric oxide[11b] was examined as a strong inner-sphere 1 e$^-$ oxidant in a final attempt to access tris-Co^{III} states of the cages. As expected, treatment of **2** with 1 atm of NO in CD_3CN resulted in immediate formation of the nitrosyl complex **7** (Scheme 3) as evident from the resulting diamagnetic ^{1}H NMR spectrum and bathochromic shifts of the Soret band and q-peak in the UV-vis spectrum of the complex (Figures S10,64).[11b] Additionally, a characteristic nitrosyl N=O stretch at 1738 cm^{-1} was observed by FTIR spectroscopy for a solid sample of **7**•4PF_6.[11b] Similar results were obtained upon treatment of **Co$_3$-1a**,**b** with NO in CD_3CN (Scheme 4). The paramagnetic ^{1}H NMR spectra of the Co^{II} cages were resolved into diamagnetic spectra (Figures 4 and S20), and changes were observed in the UV-vis spectra of the cages (Figures S69,70) that are similar to those observed upon conversion of **2** to **7**. Lastly, nitrosyl N=O stretches at 1733 and 1713 cm^{-1} were observed for **[Co^{III}NO]$_3$-1a** and **[Co^{III}NO]$_3$-1b**, respectively. Notably, the ^{1}H NMR spectrum of **[Co^{III}NO]$_3$-1a** (Figure 4) shows six aromatic resonances and splitting of the tmeda *N*CH_3 resonances into two singlets, clearly indicating retention of the cage structure.[7b] Several smaller signals are also present, which may be due to endo/exo isomerism of the nitrosyl ligands or due to partial degradation of the cage. Nevertheless, the major signals leave no doubt as to successful formation of intact **[Co^{III}NO]$_3$-1a**, and a similar ^{1}H NMR spectrum was obtained for **[Co^{III}NO]$_3$-1b** (see Figure S20).

In summary, **Co$_3$-1a**,**b** were prepared as new examples of nanocages with cobalt-porphyrin walls. The redox properties of **Co$_3$-1a**,**b** were evaluated, revealing facile reduction of these paramagnetic tris-Co^{II} cages to diamagnetic tris-Co^{I} states **Co$^{I}_3$-1a**,**b**, which are the first spectroscopically characterized Co^{I} porphyrin nanocages. In contrast, tris-Co^{III} states of the cages were harder to access, likely due to geometric constraints imposed by the 3D cage structures. However, use of the small, inner-sphere oxidant NO led successfully to the formation of **[Co^{III}NO]$_3$-1a**,**b**. Thus, Co^{I}, Co^{II}, and Co^{III} states of the cobalt-porphyrin nanocages were accessed. We expect that these fundamental redox-reactivity studies will contribute to the development of metalloporphyrin nanocages as catalysts for a variety of redox transformations.

This work was supported by the ACS Petroleum Research Fund (PRF grant #61015-DNI3).

Conflicts of interest

There are no conflicts to declare.

Notes and references

‡ Analysis of EPR line broadening is described in the SI.
§ Use of $[Me_3O]BF_4$ as a CH_3^+ source avoids introducing halide anions that would precipitate the cages from acetonitrile.

1 T. R. Cook, P. J. Stang *Chem. Rev*. 2015, **115**, 7001–7045.
2 (a) M. Yoshizawa, J. K. Klosterman, M. Fujita, *Angew. Chem. Int. Edit.* 2009, **48**, 3418–3438. (b) E. G. Percástegui, T. K. Ronson, J. R. Nitschke *Chem. Rev*. 2020, **120**, 13480–13544.
3 (a) T. N. Parac, D. L. Caulder, K. N. Raymond *J. Am. Chem. Soc.* 1998, **120**, 8003–8004. (b) M. Fujita, S. Nagao, K. Ogura *J. Am. Chem. Soc.* 1995**, 117**, 1649–1650.
4 (a) N. Kishi, M. Akita, M. Kamiya, S. Hayashi, H.-F. Hsu, M. Yoshizawa *J. Am. Chem. Soc.* 2013, **135**, 12976–12979 (b) R. J. Li, J. Tessarolo, H. Lee, G. H. Clever *J. Am. Chem. Soc.* 2021, **143**, 3865–3873. (c) L. S. Lisboa, J. A. Findlay, L. J. Wright, C. G. Hartinger, J. D. Crowley, *Angew. Chem. Int. Ed.* 2020, **59**, 11101–11107.
5 (a) W. Cullen, A. J. Metherell, A. B. Wragg, C. G. P. Taylor, N. H. Williams, M. D. Ward, *J. Am. Chem. Soc.* 2018, **140**, 2821–2828. (b) I. A. Bhat, A. Devaraj, P. Howlader, K. W. Chi, P. S. Mukherjee, *Chem. Comm.* 2018, **54**, 4814–4817. (c) Q. Q. Wang, S. Gonell, S. H. A. M. Leenders, M. Dürr, I. Ivanovic-Burmazovic, J. N. H. Reek, *Nat. Chem.* 2016, **8**, 225–230.
6 (a) V. Croué, S. Goeb, M. Sallé, *Chem. Comm.* 2015, **51**, 7275–7289. (b) S. Goeb, M. Sallé *Acc. Chem. Res.* 2021, **54**, 1043–1055.
7 (a) R. Plessius, N. Orth, I. Ivanović-Burmazović, M. A. Siegler, J. N. H. Reek, J. I. van der Vlugt *Chem. Commun.* 2019, **55**, 12619–12622. (b) K. G. Dutton, D. A. Rothschild, D. B. Pastore, T. J. Emge, M. C. Lipke *Inorg. Chem.* 2019, **59**, 12616–12624. (c) I. F. Mansoor, K. G. Dutton, D. A. Rothschild, R. C. Remsing, M. C. Lipke ChemRxiv. Cambridge: Cambridge Open Engage; 2021; This content is a preprint and has not been peer-reviewed. (d) Z. Lu, T. K. Ronson, J. R. Nitschke *Chem. Sci.* 2020, **11**, 1097–1101. (d) G. Szalóki, V. Croué, V. Carré, F. Aubriet, O. Alévêque, E. Levillain, M. Allain, J. Aragó, E. Ortí, S. Goeb, M. Sallé, *Angew. Chem. Int. Ed.* **2017**, *56*, 16272–16276
8 K. Yazaki, S. Noda, Y. Tanaka, Y. Sei, M. Akita, M. Yoshizawa *Angew. Chem. Int. Ed.* 2016, **55**, 1503–15034.
9 A. J. Plajer, F. J. Rizzuto, L. K. S. von Krbek, Y. Gisbert, V. Martínez-Agramunt, J. R. Nitschke *Chem. Sci.* 2020, **11**, 10399–10404.
10 (a) P. T. Smith, B. P. Benke, Z. Cao, Y. Kim, E. M. Nichols, K. Kim, C. J. Chang *Angew. Chem. Int. Ed.* 2018, **57**, 9684–9688. (b) P. T. Smith, Y. Kim, B. P. Benke, K. Kim, C. J. Chang, *Angew. Chemie. Int. Ed.* 2020, 59, 4902–4907 (c) A. N. Oldacre, A. E. Friedman, T. R. Cook *J. Am. Chem. Soc.* 2017, **139**, 1424–1427. (d) M. R. Crawley, D. Zhang, A. N. Oldacre, C. M. Beavers, A. E. Friedman, T. R. Cook *J. Am. Chem. Soc.* 2021, **143**, 1098–1106.
11 (a) C. Araullo-McAdams, K. M. Kadish *Inorg. Chem.* 1990, **29**, 2749–2757. (b) G. B. Richter-Addo, S. J. Hodge, G.-B. Yi, M. A. Khan, T. Ma, E. V. Caemelbecke, N. Guo, K. M. Kadish *Inorg. Chem.* 1996, **35**, 6530–6538. (c) A. M. Stolzenberg, J. S. Summers *Inorg. Chem.* 2000, **39**, 1518–1524. (d) M. K. Geno, J. Halpern *J. Am. Chem. Soc.* 1987, **109**, 1238–1240.
12 S. Durot, J. Taesch, V. Heitz *Chem. Rev.* 2014, **114**, 8542–8578.
13 A. K. Bar, S. Mohapatra, E. Zangrando, P. S. Mukherjee *Chem. Eur. J.* 2012, **18**, 9571–9579.
14 N. G. Connelly, W. E. Geiger *Chem. Rev.* 1996, **96**, 877–910.
15 T. J. Curphey *Org. Synth.* 1971, **51**, 142.